Volume 150
Number 10
21 May 2025
Pages 1963-2192

Analyst

rsc.li/analyst

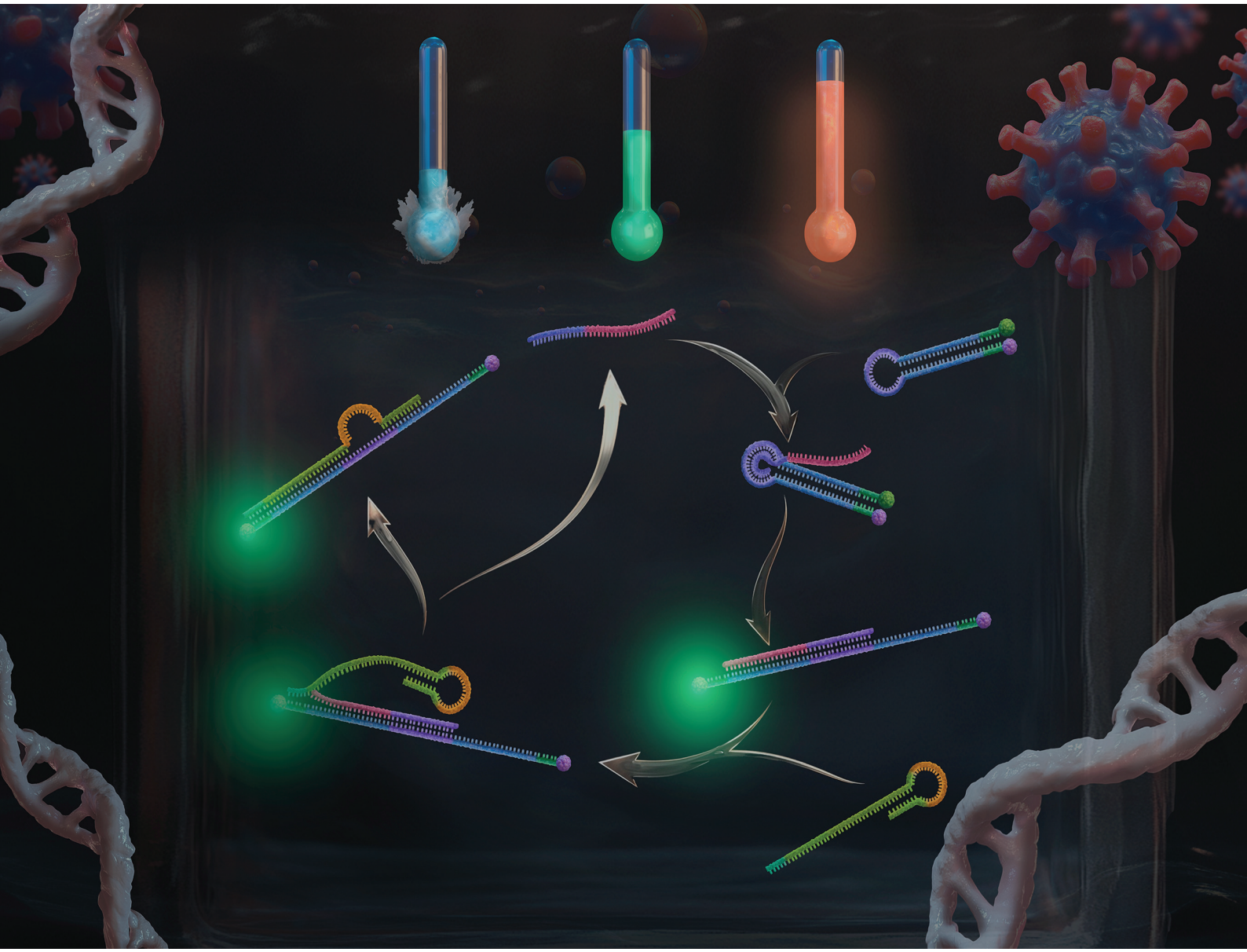

ISSN 0003-2654

ROYAL SOCIETY OF CHEMISTRY

PAPER
Jamal Daoud, Jonathan Perreault *et al.*
Enzyme-free temperature resilient amplification assay with toehold stem-loop probe

150 YEARS ANNIVERSARY

Analyst

ROYAL SOCIETY OF CHEMISTRY

PAPER

View Article Online
View Journal | View Issue

Cite this: *Analyst*, 2025, **150**, 2019

Enzyme-free temperature resilient amplification assay with toehold stem-loop probe†

Jay Bhakti Kapadia, [a] Jamal Daoud*[b] and Jonathan Perreault*[a]

Toehold mediated strand displacement reaction (TMSDR) offers a rapid, enzyme-free amplification strategy, providing advantages over traditional methods like RT-PCR, and RT-LAMP. Optimizing TMSDR can significantly enhance sensitivity in point-of-care biosensor applications for target nucleic acid detection. However, achieving optimal performance requires meticulous probe design and stringent quality control. We developed a TMSDR-based system targeting a specific SARS-CoV-2 RNA sequence through testing multiple fluorophore–quencher labeled DNA probes. Following optimization, a probe with a strategically designed: stem, loop, and optimized toehold length emerged as the most effective candidate. Displacer sequence optimization further enhanced amplification efficiency. Ensuring probe purity is crucial, as impurities elevated background noise and diminished sensitivity. This work underscores the importance of rigorous probe quality in achieving reliable and sensitive TMSDR-based viral RNA detection, paving the way for robust point-of-care diagnostic tools.

Received 12th September 2024,
Accepted 27th January 2025

DOI: 10.1039/d4an01212g

rsc.li/analyst

Introduction

Toehold-mediated strand displacement reactions (TMSDR) have emerged as potential tools in molecular diagnostics and DNA nanotechnology, enabling precise and efficient detection of specific target sequences and importantly, without the need for enzymatic amplification. The enzyme-free nature of TMSDR simplifies the detection process, reduces costs, and minimizes operational complexities, making it an attractive method for various applications. TMSDR leverages nucleic acid hybridization kinetics, which is applicable in diverse scientific fields, from enhancing molecular diagnostics to environmental monitoring methodologies.[1–5] Extensive research into the mechanistic and application-oriented aspects of TMSDR has driven the technology's development and integration into practical tools for molecular biology.[6] However, strand displacement reactions suffer with the sensitivity and hence an additional nucleic acid strand is used to enhance the target recycling and amplify signal.[7,8] The additional nucleic acid strand is usually termed as displacer strand or fuel strand.[7–9]

Fig. 1A provides a comprehensive depiction of the amplification schematic, emphasizing the pivotal role and concentration of the displacer strand. The design and concentration of the displacer strand are crucial for the overall dynamics and outcome of TMSDR.[8,10,11] The specificity, efficiency, and sensitivity of TMSDR largely depend on the structural attributes of the probe and displacer strands.[8] Optimization in this area has led to remarkable improvements in reaction kinetics, enhancing sensitivity and specificity within detection assays.[12]

Moreover, this paper demonstrates the potential utility of TMSDR system in point-of-care biosensors, presenting a significant advancement over traditional molecular diagnostics such as reverse transcription quantitative PCR (RT-qPCR), loop mediated isothermal amplification (LAMP) and hybridization chain reaction (HCR).[13–16] Traditional techniques often suffer from limitations such as the need for specialized equipment and enzymes in RT-qPCR.[17] LAMP also requires enzymes, which increase cost and limits shelf-life, but also suffers from unreliability and frequent false positives.[18] HCR is based on TMSDR and, while it is somewhat leaky,[19] it offers several advantages, including its enzyme-free nature, the ability to target both DNA and RNA, eliminating the need for reverse transcription, requiring only two DNA strands (metastable hairpin like stems), and producing results within 3 hours with high specificity, even in detecting single nucleotide polymorphisms (SNPs).[19–21] Advances in biosensor technology leveraging TMSDRs open new pathways for sensitive and specific genetic analysis, paving the way for innovative approaches to diagnosing and addressing genetic conditions.[22] Additionally, TMSDRs role in creating dynamic and programmable molecular systems highlights its adaptability and potential for addressing diagnostic challenges.[2,3,23] The develop-

[a]*INRS-Armand Frappier Institute-531, Boul. Des Prairies, Laval, QC, H7 V 1B7, Canada. E-mail: jonathan.perreault@inrs.ca*
[b]*Galenvs Sciences-6750 Rue Hutchison, Montreal, QC, H3N 1Y4, Canada. E-mail: jdaoud@galenvs.com*

† Electronic supplementary information (ESI) available. See DOI: https://doi.org/10.1039/d4an01212g

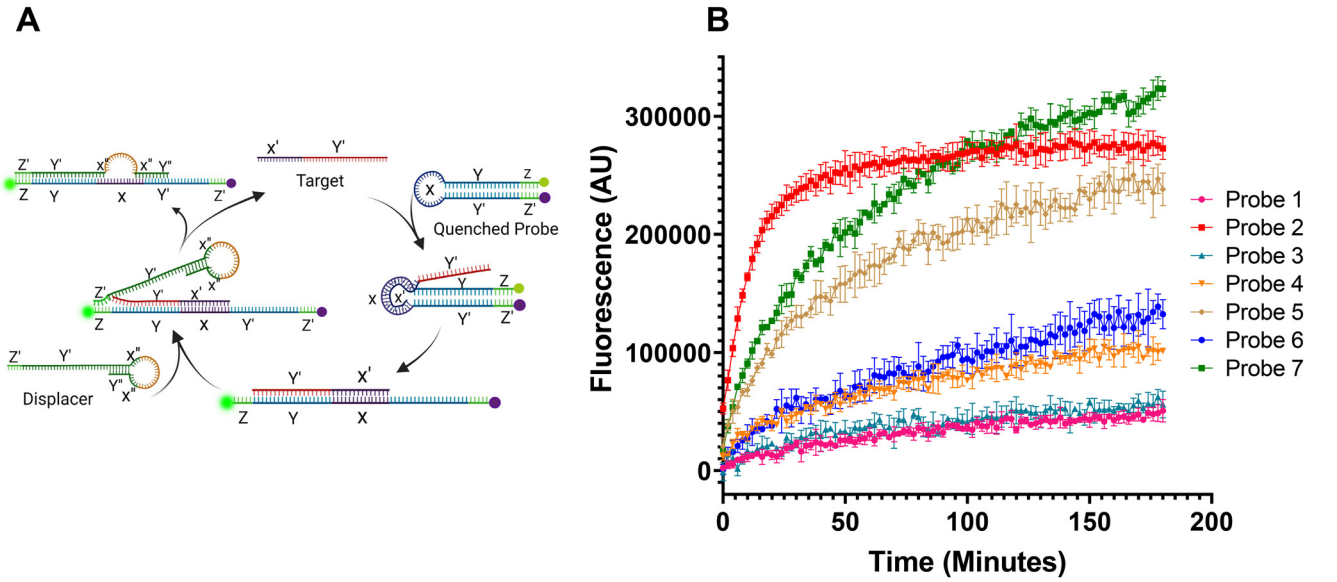

Fig. 1 Probe characterizations in the presence of SL target. (A) Schematic representation of enzyme-free amplification by toehold mediated strand displacement reactions. (B) Graph illustrates comparison of different probes in the presence of excess target (10× more compared to the concentration of the probe (0.05 μM)). The probes were designed against SARS-CoV-2 viral RNA target (variant B.1.617.2). The assays were performed in n = 3 replicates, and mean values are plotted. Standard deviations were used for error bars.

ment of such systems, capable of complex behaviors and programmable functionalities, presents novel diagnostic solutions that are not only innovative but also highly adaptable to various biological contexts.[3,20]

As TMSDR technology continues to mature, its capacity for enhancing molecular diagnostics through the strategic design of probe and displacer strands becomes increasingly evident. This study contributes to the expanding body of knowledge on TMSDR, offering insights into how displacer strand design can be optimized. Furthermore, the potential of TMSDR is demonstrated using a DNA oligo corresponding to SARS-CoV-2 sequence. To further improve the general applicability of hairpin-type toeholds we explored several avenues of probe and displacer strand design, focusing on how subtle modifications can dramatically enhance TMSDR-based assays, such as resilience to temperature. Various displacer strands and probes were characterized to devise simple rules to permit signal amplification and specificity improvement including importance of oligonucleotide purity. We detail certain structural modifications, notably the introduction of partial complementarity to the loop domain of the probe, which significantly enhance signal detection, marking a significant stride towards the refinement of TMSDR as a molecular diagnostics tool.

Materials and methods

Probe selection and design

To detect target nucleic acids in the environment using strand displacement reactions, conserved regions were identified on each lineage of SARS-CoV-2 using the GISAID database.[24,25] Sequences from lineages including B.1.617.2, alpha, beta, gamma, delta, and omicron were sub-grouped and analyzed. Conserved regions of 70 nucleotides were identified using ClustalW for their potential to form hairpin domains, comprising a single-stranded loop and a base-paired stem. These regions were chosen based on their stability and the adequacy of their melting temperatures to ensure effective probe binding.

The ViennaRNA package's RNApfold tool was used to estimate the probability of unpaired nucleotides within 15-nucleotide segments of the selected sequences.[26,27] A threshold of ≥60% unpairing likelihood was set as a placeholder to identify accessible regions. These accessibility profiles were utilized to compute optimal and suboptimal secondary structures of hybridization between our target sequences and each corresponding viral genome within a lineage using RNAplex.[26,27]

Sequences exhibiting a minimum free energy (MFE) of less than −30 kcal mol^{-1} were selected for further consideration. This energy threshold was chosen to ensure a high probability of stable probe–target hybridization under typical physiological conditions. Additionally, only hairpins with a melting temperature (T_m) greater than 40 °C were retained to ensure structural integrity and functionality at room temperature and above.[26,27]

Using RNAplex, the interaction of these hairpin probes with the human genome and other respiratory viral genomes was assessed to evaluate specificity.[26] Probes were selected based on their maximum hybridization interaction with the COVID-19 genome and minimal interaction with the human genome and other viral genomes, ensuring high specificity.[24,26,27]

The selected probes, initially comprising target sequences from the Orf1a, Orf8, M, and S genes of the B.1.617.2 lineage, were synthesized and their hairpin structures tested against corresponding target oligonucleotides (Table S1†).

Displacer design

To achieve optimal signal amplification and minimal non-specific interaction, a series of displacer strands were designed and synthesized. The selection process for these displacer strands focused on maximizing their binding specificity to the secondary toehold region of the probe while preventing non-specific interactions. The initial design of the displacers was based on their theoretical ability to bind the exposed toehold region of the probe effectively. Several variations were synthesized, each with distinct structural characteristics to explore their impact on strand displacement kinetics and amplification efficiency. These variations included adjustments in sequence length and composition to enhance specificity. Sequences of the displacer strands are provided in Table S1.†

Oligonucleotide synthesis and purification

The DNA oligonucleotide for the probe, containing the stem-loop forming sequence and FAM/BHQ-2 modifications (Fig. S1†), was synthesized in-house (Galenvs Sciences) using a K & A H-16 DNA synthesizer (Sierra Biosystems) and standard phosphoramidite chemistry. The probe oligonucleotide was purified using reverse-phase HPLC on a Gilson HPLC system. The non-modified target and displacer oligonucleotides were purified using Phenomenex QSP reverse-phase cartridges. All oligonucleotides were purified to ensure at least 85% purity measured by reverse phase analytical HPLC (Waters ARC HPLC).

Probe preparation in thermal cycler

The probe oligonucleotide was diluted to 50 nM in isothermal amplification buffer II (NEB) with 4 mM $MgSO_4$ and subjected to a thermal protocol using a T1000 Thermal Cycler (Bio-Rad): 95 °C for 5 minutes, 50 °C for 10 minutes, and 37 °C for 10 minutes. Proper folding of the probe was confirmed through the absence of signal in negative control reactions during the TMSDR assay. The folded probe was stored at 4 °C for short-term use to enhance stability and minimize denaturation.

Enzyme free amplification assay

TMSDRs were carried out in a 50 μL volume using isothermal amplification buffer II (NEB) supplemented with 4 mM $MgSO_4$ (NEB). Unless otherwise stated, the reaction mixture contained 50 nM of the hairpin DNA probe, either 1 nM or 5 nM of the target nucleic acid, and in absence or with various concentrations of the displacer oligonucleotide. Reactions were incubated at room temperature (~22 °C) unless otherwise stated. Amplification was monitored using a SpectraMax iD3 microplate reader (Molecular Devices) with excitation and emission wavelengths set at 490 nm and 530 nm, respectively, to detect the fluorescence signal from FAM and BHQ-2 labeled probes. Reactions were carried out in 96-well black clear-bottom plates (NEST). Fluorescence readings were taken at 2-minute intervals throughout the reaction.

Results

Initial probe designs and selection

Seven TMSDR probes were designed to target different regions of the SARS-CoV-2 B.1.617.2 variant genome. Fig. S1† schematically depicts the design of each probe, highlighting the target-specific loop domain and the stem-loop structure (Fig. S1†).[26]

The binding affinity of the designed probes to their respective targets was assessed by incubating each probe with a 10-fold excess (0.5 μM) of its fully complementary target sequence (same length, SL target). Under this condition, the SL target hybridizes with the entire loop domain of the probe, and then to the 5′ side of the stem region. This experimental setup allows for the evaluation of direct probe–target interactions without the initiation of the secondary strand displacement reaction by the displacer strand. Fig. 1B displays the fluorescence signal over time for each probe. The observed increase in fluorescence reflects the binding of the SL target to the probe, leading to the unquenching of the fluorophore. Probe 2 exhibited the fastest rise to a plateau phase, suggesting a higher binding affinity and faster binding kinetics compared to the other probes (Fig. 1B and Table S2†). While probe 7 reached a higher final fluorescence intensity towards the end of the assay, its slower approach to the plateau phase indicated slower binding kinetics compared to probe 2 (Fig. 1B and Table S2†). Although it might be coincidental, we noticed that all the probes without internal base pairing in their loop domain (probe 2, 5, 6 and 7) have higher plateaus compared to probes with predicted base pairs in their loop domain (probe 1, 3 and 4) (Fig. S1 and Table S2†). Based on its superior binding kinetics, probe 2 was selected for further investigation in TMSDR amplification reactions using a truncated target (Trn target), which exposes a 5-nucleotide toehold for displacer binding and subsequent signal amplification.

Probe optimization

To further characterize the performance of probe 2, a series of experiments were conducted to investigate the impact of target toehold length, stem length, and point mutations on target binding (Fig. 2). The tolerance of probe 2 to point mutations within the target sequence was assessed by introducing single nucleotide mismatches at various positions along the target. Fig. 2A illustrates the design of probe 2 and indicates the positions where mutations were introduced in the target sequence. The graph in Fig. 2A shows the fluorescence signal resulting from the interaction of probe 2 with each mutant target. The kinetic data is presented in Table S2† extracted from Fig. 2A. Notably, a mutation at the 15th nucleotide, located at the junction between the loop and stem domains, exhibited the most significant impact on target binding, leading to a substantially

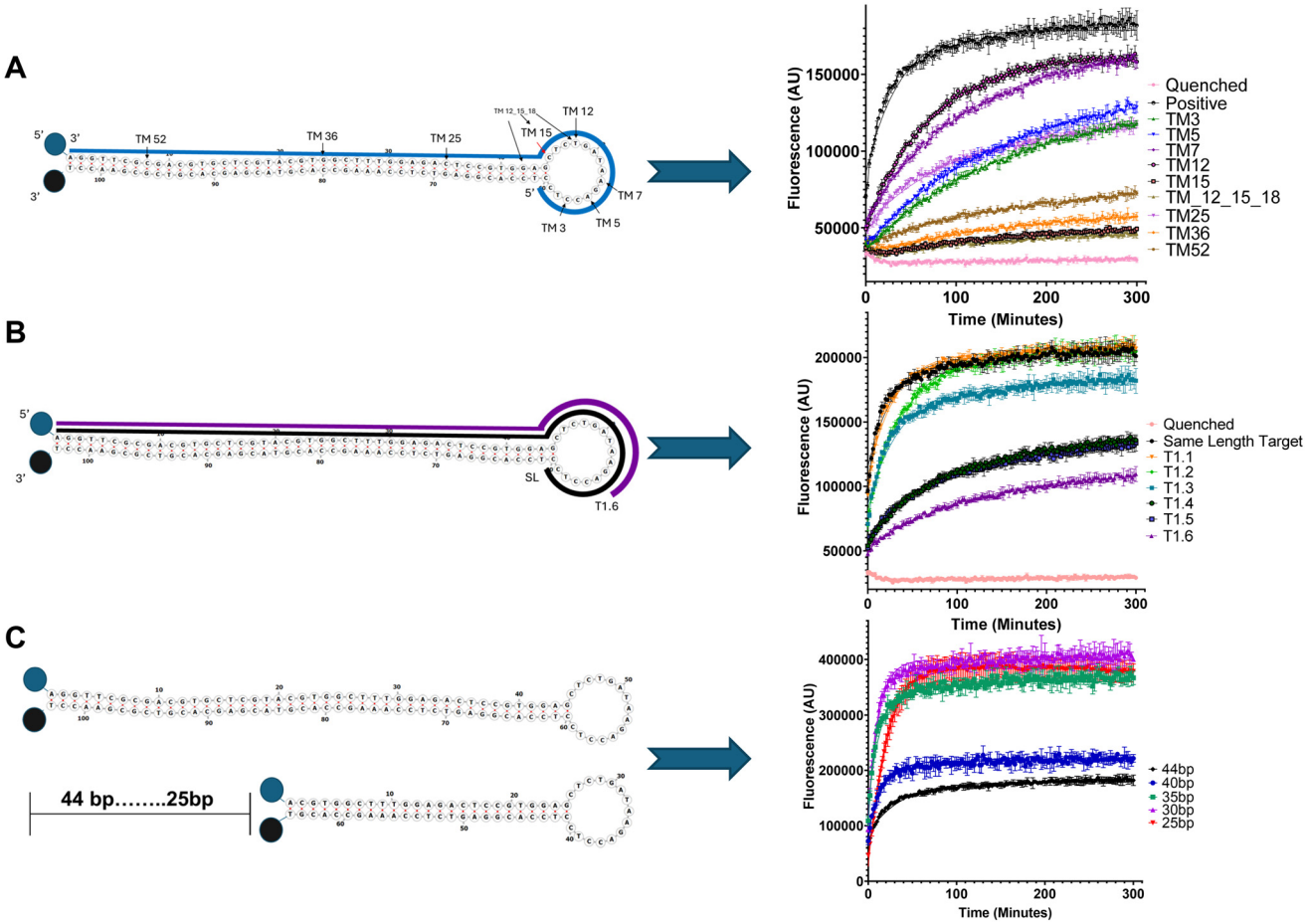

Fig. 2 Characterization of probe-2 with different targets to assess tolerance to different mutations as well as optimal toehold length for the target. All the assays were performed for 5H at room temperature. (A) Probe-2 was assayed with different mutant targets. As illustrated in the picture of the probe, all the mutation positions are marked by the arrow on the structure. TM3 designates mutation on 3rd nucleotide of the target sequence (blue strand) and so on. The graph illustrates the assay that was performed at room temperature in 96 well plates and FAM and BHQ-1 was used as fluorophore and quencher. (B) Probe 2 was assayed in the presence of different toehold length of the target sequences. Different target sequences termed T.1, T1.2 ... refers to one nucleotide truncations at 5′ end. The graph illustrates the assay in the presence of same length target. (C) This assay was performed with five different probes of the same sequence. Each probe has different stem length ranging from 44 bp to 25 bp. The same length target was used for this assay. The assays were performed in n = 3 replicates, and mean values are plotted. Standard deviations were used for error bars.

reduced fluorescence signal. This finding suggests that the nucleotide directly adjacent to the stem-to-be-opened plays a crucial role in the specificity of probe 2 and highlights its potential for detecting single nucleotide polymorphisms (SNPs). Note that the probes were also tested in the presence of human genomic DNA to evaluate for non-specific binding and were not found to be influenced by the presence of such DNA (Fig. S2†).

To investigate the influence of target toehold length on probe 2 performance, a series of truncated targets were designed with varying lengths of the single-stranded toehold region. Fig. 2B depicts the structure of probe 2 with a target truncated from its 5′ end, resulting in toehold lengths ranging from 14 nucleotides (T1.1) to 9 nucleotides (T1.6). The graph in Fig. 2B compares the fluorescence signals obtained with each truncated target and the full-length (same length, SL) target as a control. The results indicate that T1.1, T1.2, and T1.3, with toehold lengths of 14, 13, and 12 nucleotides respectively, exhibited similar fluorescence intensities within the error range, suggesting that these lengths provide sufficient binding affinity for probe 2. However, a significant decrease in fluorescence was observed for T1.4, T1.5, and T1.6 (11, 10, and 9 nucleotides respectively), indicating that toehold lengths below 12 nucleotides result in noticeably reduced binding. More precisely the analysis of different kinetic values emphasize on the fact that the K_{obs} and plateau decrease as the toehold length is reduced (Table S3†). This finding is particularly noteworthy as it challenges the common assumption that toehold lengths exceeding 6 nucleotides are sufficient for optimal binding in TMSDR systems,[6,10] which appears to differ in the context of stem-loop toeholds.

To investigate the influence of stem length on probe 2 performance, a series of truncated probes were designed with progressively shorter stem domains. Fig. 2C illustrates the struc-

ture of probe 2 and indicates the region where truncations were made, resulting in probes with stem lengths ranging from 40 base pairs (bp) (probe 2-1) to 25 bp (probe 2-4). These truncated probes were assayed in the presence of a 10-fold excess of the SL target (0.5 μM), to assess the effect of stem length on target binding affinity. As the stem length decreased, the fluorescence intensity increased (Fig. 2C). Probe 2 with the full-length stem (44 bp) exhibited the lowest fluorescence and probes showed progressively higher fluorescence levels as the stem sized was decreased. Although the fluorescence intensities and plateau values for probe 2-2, 2-3, and 2-4 were within a similar range, probe-2-4 was selected for further TMSDR amplification studies due to its shortest stem length, offering potential economic advantages and reduced steric hindrance in the context of point-of-care (POC) devices (Table S4†).

Amplification and displacer optimization

To illustrate the mechanism underlying the enzyme-free amplification process, Fig. 1A provides a scheme of the TMSDR reactions. Initially, the probe exists in a closed stem-loop conformation, with the fluorophore quenched by the quencher due to their close proximity (Fig. 3AI). This state represents the baseline fluorescence level in the absence of the target. The truncated target, designed to be complementary to the loop region of the probe, binds to the probe loop. This specific interaction triggers the first strand displacement reaction, where the target hybridizes with the 5′ strand of the stem, disrupting the stem-loop structure and exposing the secondary toehold region at the 5′ extremity of the probe (Fig. 3AII). This transition from a closed to an open conformation marks the activation of the probe. The displacer strand, engineered to be complementary to the exposed secondary toehold, binds to the probe. Although the displacer cannot initiate the opening of the probe by itself, its binding is crucial for maintaining the probe in its open, activated state. The binding of the displacer triggers a second strand displacement reaction, releasing the target from the probe while the displacer remains bound. This ensures that the probe remains in its open conformation, with the fluorophore unquenched and generating a detectable fluorescence signal (Fig. 3AIII). The released target, now free in solution, can bind to another probe molecule in its initial closed state, initiating a new cycle of probe activation, strand displacement, and target release (Fig. 1A). This continuous recycling of the target and the accumulation of open probes with unquenched fluorophores result in amplification of the fluorescence signal, enabling detection of the target nucleic acid at concentrations below the detection threshold of the apparatus used.

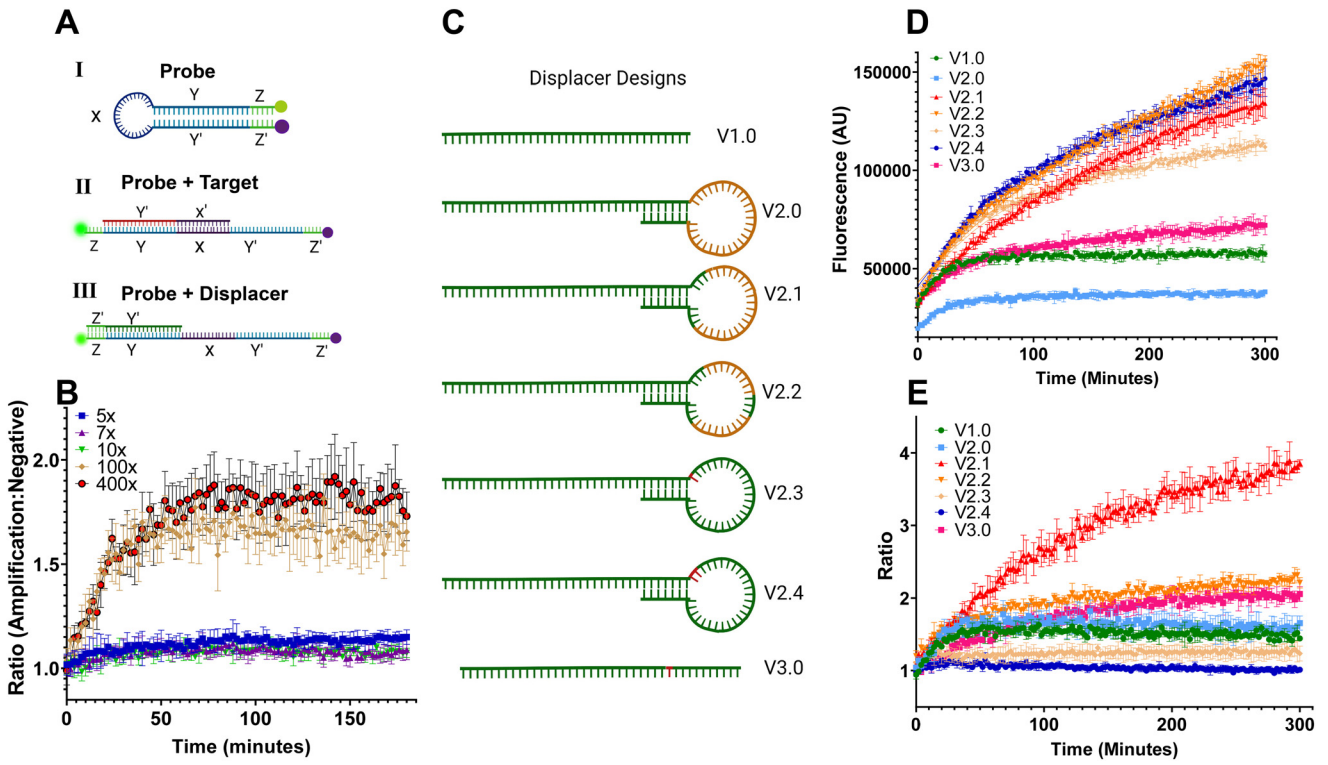

Fig. 3 Displacer optimization for enhanced TMSDR assay performance. (A) Schematic representation of quenched probe, probe bound by target and probe bound by displacer V1.0. (B) Different concentrations of displacer V1.0 comparison. (C) This schematic depicts the various displacer designs investigated for optimization in the TMSDR assay. (D) This figure illustrates the raw fluorescence intensity profiles generated during the TMSDR assay using different displacer designs. Each curve represents the fluorescence intensity over time for a specific displacer. (E) This figure shows the signal-to-noise ratio calculated for each displacer design. The ratio is determined by dividing the target amplification signal (D) by the negative control signal (probe + 100× displacer). A higher ratio indicates improved assay sensitivity and specificity. The assays were performed in n = 3 replicates, and mean values are plotted. Standard deviations were used for error bars.

Initial assays at low concentrations of displacer V1.0 were carried out in the presence of 5 nM Trn target as illustrated in Fig. 3B. Initially, with 150 nM (5× the probe concentration) did not show any amplification even up to 500 nM (Fig. 3B). Concentration of displacer strand needed to be increased to 5 μM (100× the probe concentration) in order to favour displacer binding with the activated probe in the presence of Trn target (Fig. 3B).

To improve displacer design to enhance TMSDR amplification efficiency, a series of displacer sequences with varying lengths and complementarity were designed and evaluated (Fig. 3C). The initial displacer (displacer V1.0) exhibited poor signal amplification and high background noise due to non-specific interactions with the probe in the absence of the target (Fig. 3B, C and Fig. S3B†).

To address the limitations of displacer V1.0, a second generation of displacers (displacer V2.0 series) was designed with modifications aimed at eliminating undesired binding and increasing the ability of the displacer to recycle the target to improve amplification efficiency (Fig. S3C–E†). These modifications included alterations in length and sequence composition to extend complementarity for the loop toehold region and the 3′ side of the probe stem. Displacers V2.3 and V2.4 represent particularly innovative approaches, utilizing the full-length loop domain sequence of the SL target to take advantage of the fact that a single nucleotide mismatch at the 15th position almost completely blocked the target ability to displace the probe (Fig. 2A). This design aimed to leverage the high binding affinity of the SL target while preventing complete hybridization and maintaining accessibility of the toehold for strand displacement (Fig. S3F and G†). Displacer V3.0 further explored this concept by reducing the complementary stem region to 9 nucleotides, potentially keeping the V2.3 and V2.4 displacer's ability to initiate strand displacement, while reducing background. Displacer V3.0 included an additional mismatch at the 14th nucleotide to further investigate the impact of mismatches on displacer function (Fig. S3H†).

The performance of the different displacer variants was evaluated in TMSDR amplification using probe 2-4 and the truncated target. Fig. 3D displays the raw fluorescence signal generated by each displacer over time, providing a direct comparison of their amplification kinetics. Displacer variants 2.1, 2.2, 2.3, and 2.4 exhibited similar fluorescence intensities, suggesting comparable amplification capabilities.

However, to account for potential background noise, Fig. 3E presents the ratio of the amplification signal to the negative control signal (probe + displacer without target) for each displacer variant. This ratio provides a more accurate measure of the true amplification efficiency and specificity. Notably, displacer V2.1 demonstrated the highest amplification-to-negative control ratio, indicating superior performance with minimal background noise. This result highlights the importance of minimizing background signal for achieving optimal amplification and specificity in TMSDR reactions. In other words, the ability of the displacer to compete with the target needs to be carefully balanced. We have made sure that probe 2-4, its target and the displacer V2.1 actually behaved as suggested by our fluorescence assay by evaluating TMSDR amplification products on a 12% native polyacrylamide gel (Fig. S4†). Expected quenches/unquenched band pattern was observed for each sample.

To further validate the design parameters, we extended our study to include TMSDR amplification utilizing probe 6, which also demonstrated successful performance using these criteria (Fig. S5†). This additional experiment serves as another example of the TMSDR system with a different target sequence and reinforces the robustness of the probe and displacer design parameters. Moreover, to further assess the specificity of TMSDR, an identical assay using a mutant truncated target with a 15th nucleotide point mutation was conducted, which showed no amplification even after 24 hours (Fig. S6†). We also conducted our assay with an RNA target (Fig. S7A†), demonstrating the assay's capability to work with both target types.

To assess the critical role of probe purity in TMSDR performance, we compared the performance of the same probe sequence obtained commercially (polyacrylamide gel electrophoresis [PAGE]-purified) to a further purified version generated in-house using high-performance liquid chromatography (HPLC). While the commercially obtained probe underwent PAGE purification, our in-house HPLC analysis revealed the presence of residual impurities. Fig. 4A depicts the HPLC traces of the commercially obtained probe (solid blue line) and the in-house purified probe (solid red line). The commercially obtained probe shows a distinct peak profile compared to the purified probe, suggesting the presence of residual impurities despite the initial PAGE purification. The impact of probe purity on the TMSDR assay is illustrated in Fig. 4B and C. Fig. 4B shows the results using the commercially obtained probe (with only PAGE purification). Here, the target amplification curve is depicted in red, while the negative control curve is shown in green. The target signal is partially masked by high background noise (green curve), potentially leading to misinterpretation due to difficulty distinguishing specific binding from non-desired interactions. In contrast, Fig. 4C showcases the assay with the in-house purified probe. Here, the target amplification curve is also depicted in red, and the negative control curve is shown in green. A clear distinction is observed between the target signal and the negative control, with minimal background noise (green curve). This indicates improved assay sensitivity and specificity due to reduced non-desired interactions caused by remaining impurities in the commercially obtained probe. Fig. 4D quantitatively compares the performance of the purified and non-purified probes. The ratio of target signal to negative control fluorescence intensity is significantly higher for the in-house purified probe (red curve) compared to the commercially obtained probe (blue curve). The fact that a PAGE purified oligonucleotide had impurities that hampered our amplification assay emphasizes the critical role of stringent probe quality control and purity and its impact on TMSDR.

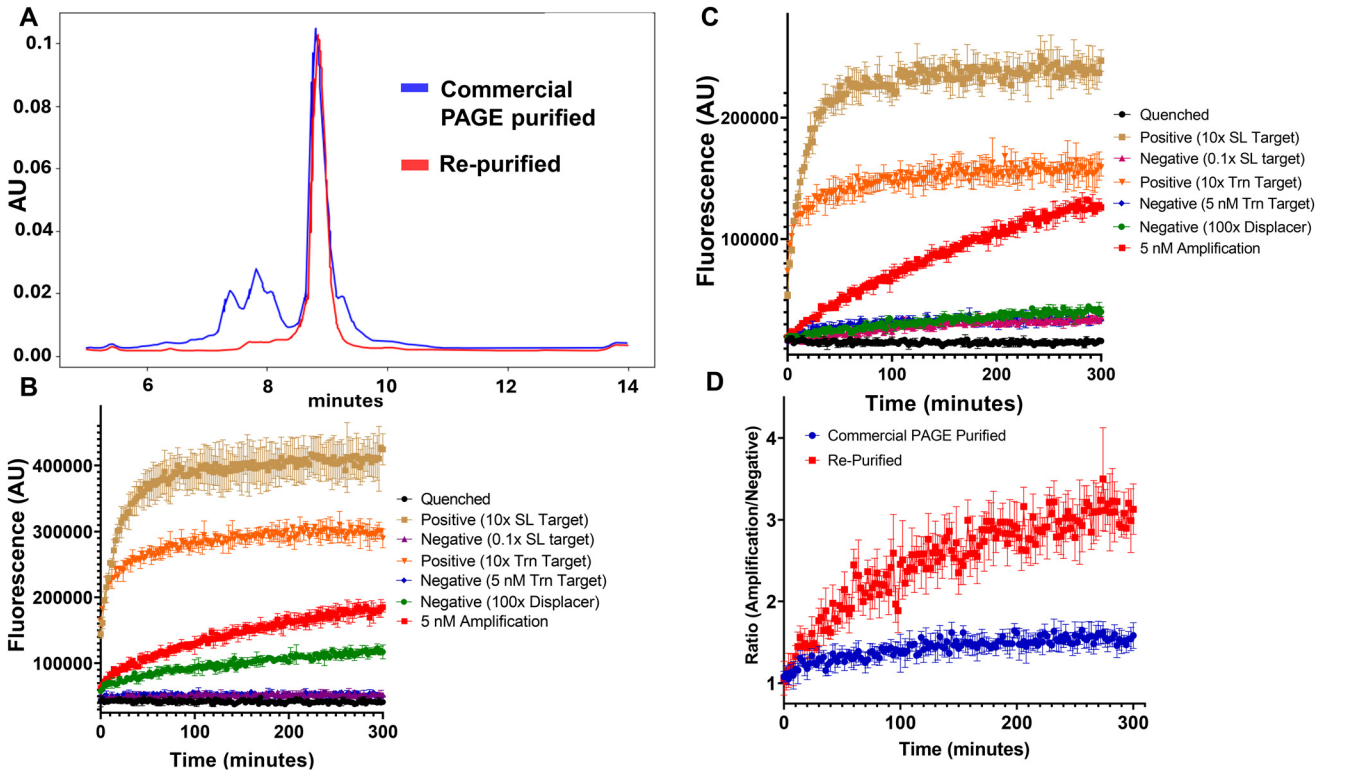

Fig. 4 Impact of probe purity on TMSDR performance. (A) HPLC analysis reveals a difference in peak profiles between the commercially obtained probe (blue curve) and the in-house purified probe (red curve). This comparison suggests the presence of impurities in the commercially obtained probe. (B) TMSDR assay using the commercially obtained probe (without purification) exhibits high background noise (green curve) that partially masks the target signal (red curve). This could lead to misinterpretation of results. (C) TMSDR assay using the in-house purified probe demonstrates a clear distinction between the target signal (green curve) and the negative control (red curve), indicating minimal background noise and improved assay sensitivity. (D) The ratio of target signal to negative control fluorescence intensity is significantly higher for the purified probe compared to the non-purified probe. This highlights the importance of probe purity for achieving reliable and sensitive TMSDR results. The assays were performed in n = 3 replicates, and mean values are plotted. Standard deviations were used for error bars.

Following the selection of probe 2-4 and displacer V2.1, amplification assay was performed using all the controls. Also, the assay was performed at different temperatures to showcase the robustness of the probe (Fig. 5A–C).

The results demonstrate a clear and robust increase in fluorescence signal over time for the amplification reaction (shown as the red curve in Fig. 5A–C), indicating successful target amplification over the 24 hours duration of the assay. All control reactions exhibited significantly lower fluorescence levels, confirming the specificity of the amplification process and the absence of significant background noise. Moreover, the same assay was conducted at lower temperature (5 °C) with all relevant controls (Fig. 5A). The assay was performed by incubating the well plate in a refrigerator and taking readings every 15 minutes. The last read was taken after overnight incubation of the plate in the refrigerator (Fig. 5A). An identical assay was performed at elevated temperature (35 °C) to demonstrate the robustness and stability of the hairpin probe and amplification assay (Fig. 5C). Similarly, DNA target dissolved in viral transport media and viral lysis buffer (Fig. S7B†), could be successfully detected confirming our assay's effectiveness in conditions that mimic in-field experimental settings.

Discussion

This study aimed to develop and optimize an enzyme-free, isothermal nucleic acid amplification system based on TMSDR. Through a series of experiments, we designed and characterized a panel of TMSDR probes targeting the SARS-CoV-2 B.1.617.2 variant genome. A comprehensive analysis was conducted to assess the impact of various factors, including target binding affinity, toehold length, stem length, and displacer design, on amplification efficiency.

One key finding emerged from the investigation of displacer sequences, while all displacers successfully initiated strand displacement and triggered amplification, displacer V2.1 exhibited superior performance in terms of signal-to-noise ratio. Displacer V2.1 was designed to have partial complementarity to the loop domain of the probe. This partial loop binding is hypothesized to facilitate more efficient release of the target strand following the second strand displacement event. By interacting with the loop domain, displacer V2.1 may prevent the re-hybridization of the target to the probe, thereby promoting its availability for subsequent rounds of amplification with naïve probes.

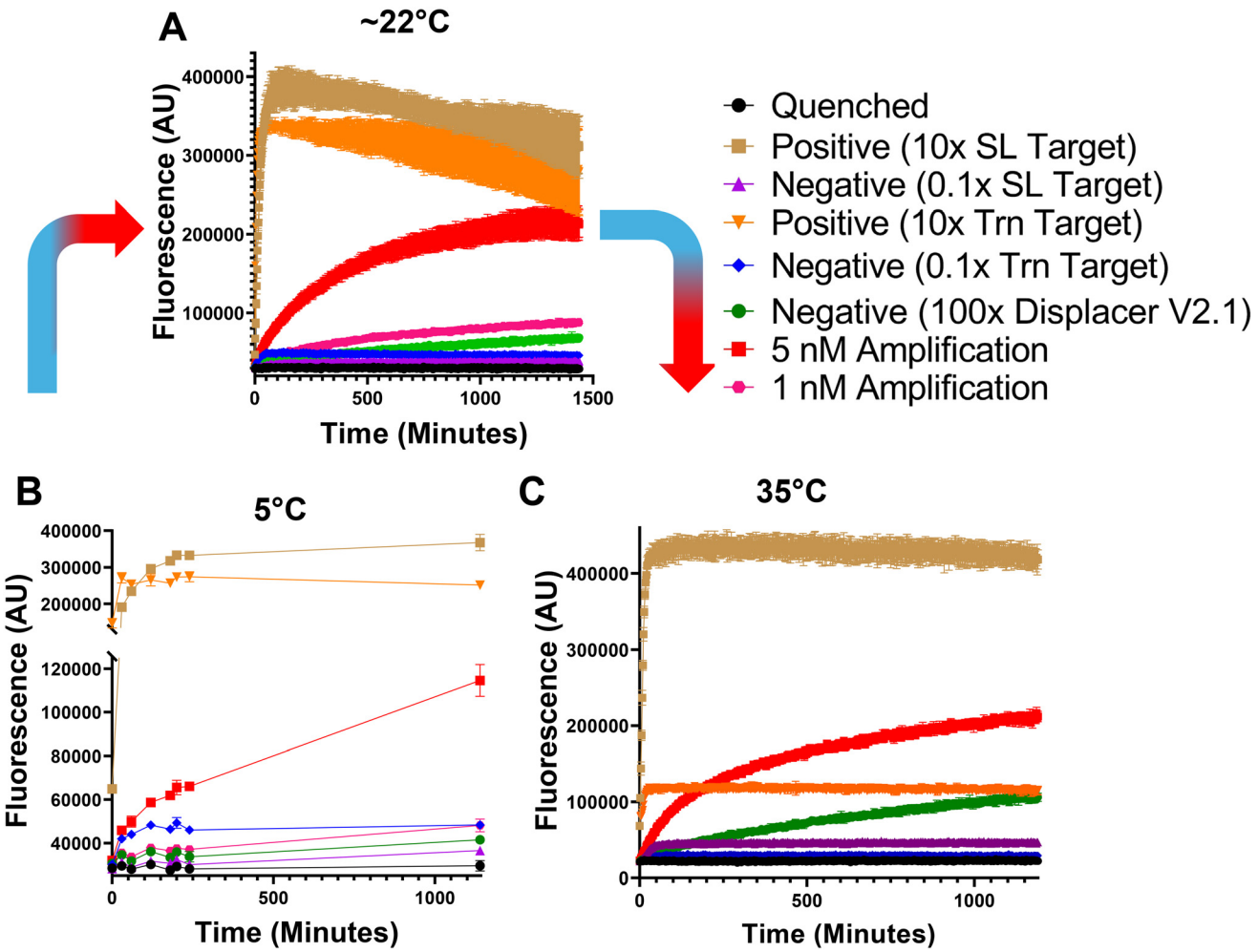

Fig. 5 TMSDR amplification assay at various temperatures. (A) TMSDR amplification assay was performed at room temperature (~22 °C) and the readings were taken every 2 minutes for the period of 24 hours. (B) TMSDR amplification assay was performed at 5 °C and the readings were taken every 30 minutes in the span of 270 minutes. Last reading was taken after overnight incubation at 5 °C. (C) TMSDR amplification assay was performed at 35 °C and the readings were taken every 2 minutes for 24 hours. The assays were performed in n = 3 replicates, and mean values are plotted. Standard deviations were used for error bars.

It is worth noting that displacer V2.2 also contained sequences complementary to the loop domain of the probe. However, the higher degree of complementarity of V2.2 compared to V2.1 resulted in increased background noise (Fig. 3D and Fig. S3C and D†). This observation highlights the importance of a balanced design for the displacer sequence. While partial loop binding appears to enhance target release and amplification efficiency, excessive complementarity can lead to unwanted interactions (*i.e.* in absence of target) and increased background signal. Still, to simplify design, exploration of displacer design led to the investigation of displacer V2.3, which is identical to the full-length target sequence but contains a single nucleotide mismatch at the 15th position. Although V2.3 did not perform as well as V2.1, such a simple approach of displacer design based on specific target-toehold mismatches may remain useful in some settings. Further investigation into incorporating additional mutations or optimizing the position of the mismatch could potentially lead to the development of simpler and more efficient displacers (Fig. S3E–G†).

In parallel, our investigation into the effect of target toehold length on probe 2 binding revealed an important insight. Contrary to the common assumption that toehold lengths exceeding 6 nucleotides are sufficient for optimal binding affinity in TMSDR systems, we observed that a toehold length of at least 12 nucleotides was necessary for efficient binding and subsequent strand displacement with our probe design.[2,10,11,28,29] This finding underscores the context-dependent nature of optimal toehold length and highlights the influence of factors such as the length of the incumbent strand and the overall length of the strand displacement reaction. As our system involved a relatively long strand displacement reaction (>20 bp), a longer toehold was required to provide sufficient binding stability for the invading strand to initiate and complete the displacement process.[1,10,11,23,28]

A noteworthy feature that emerged during the development process was the assay's adaptability to temperature variations.

The TMSDR assay was subjected to a range of temperatures, and it functioned as expected at both 5 °C and 35 °C (Fig. 5A and C). This highlights the resilience of the hairpin probe structure and underscores the assay's durability. This durability could potentially lay the groundwork for point-of-care (PoC) devices that are not dependent on temperature. Additionally, the TMSDR assay demonstrated effective performance in viral transport media (VTM) directly, allowing the nucleic acid extraction step to be skipped. This simplification enhances the process for point-of-care settings by reducing the number of steps required for the assay and enabling faster processing. Since the assay also functions effectively in lysis buffer, it eliminates the need for elution and cleanup of the sample. Moreover, lysis buffer contains chaotropic agents and detergents, which showcases the compatibility and robustness of the TMSDR assay.

While the developed TMSDR amplification system highlights several key aspects to take inconsideration and demonstrates promising features for enzyme-free and isothermal nucleic acid detection based on stem-loop toeholds, it is important to acknowledge its limitations regarding the limit of detection (LoD). Compared to highly sensitive techniques such as RT-PCR and RT-LAMP, which can achieve LoDs in the range of single-digit copy numbers, the current TMSDR assay requires further optimization to reach levels of sensitivity useful for most diagnostic applications.[15,18,30]

Hybridization chain reaction (HCR) is another isothermal amplification technique that shares some similarities with TMSDR system developed in this study.[13,31] Both methods rely on the principle of strand displacement and can achieve signal amplification without the need for enzymes or thermal cycling. However, HCR systems can be susceptible to "leakiness", resulting in higher background noise due to unintended initiation of the amplification cascade in the absence of the target.[32] This background noise can limit the sensitivity and specificity of HCR assays, particularly for low-abundance targets.[5]

The results of this study, particularly the comparison of different displacer designs (Fig. 3C), highlight the critical importance of minimizing background noise in TMSDR amplification. Displacer V1.0, which exhibited high background signal, led to poor amplification efficiency, and reduced sensitivity. In contrast, displacer V2.1, with its optimized design and minimal background noise, achieved significantly higher amplification and improved specificity. These findings underscore the need to carefully consider displacer design and optimize reaction conditions to suppress background noise and ensure efficient and reliable TMSDR amplification. Furthermore, the successful use of probe 6 with a different target sequence further solidifies the assay parameters and displacer design principles, demonstrating the versatility and robustness of the TMSDR system (Fig. S5†).

Furthermore, we highlight the critical importance of probe purity for achieving reliable and sensitive results in TMSDR assays (Fig. 4). Our comparative analysis between a commercially obtained PAGE-purified probe and an in-house purified version using HPLC highlights the significant impact that residual impurities can have on assay performance. While commercially available purification methods such as PAGE are widely used and can be beneficial, our results suggest that they may not be sufficient to ensure the optimal quality required for TMSDR applications. The HPLC analysis revealed distinct peak profiles (Fig. 4A), indicating the presence of residual impurities in the commercially obtained probe, despite undergoing PAGE purification (Fig. 4A). These impurities are likely to contribute to non-specific interactions during the TMSDR assay, leading to elevated background noise and potentially masking the target signal (Fig. 4B). This highlights a critical issue: even high-end commercial purification methods may fall short of removing all impurities, which can adversely affect the functionality and sensitivity of the assays. Our findings extend beyond the specific context of this study and have broader implications for researchers employing HCR and similar assays that rely on oligonucleotide probes.[21,29,31–33] Here, oligonucleotide purity is paramount for ensuring assay specificity and sensitivity. Leaking or non-specific signal observed in HCR assays could be attributed not only to probe design but also to the presence of impurities in the synthesized oligonucleotides.[33] Therefore, stringent quality control measures, potentially including analytical HPLC trace should be implemented to guarantee reliable data from strand displacement reactions.

This study successfully developed and optimized a TMSDR amplification system for enzyme-free and isothermal detection of nucleic acids. Through careful design and optimization of the probe (probe 2-4) and displacer (displacer V2.1), the TMSDR assay achieved efficient target amplification with minimal background noise. The investigation of target toehold length, stem length, and mutation tolerance provided valuable insights for optimizing probe performance and highlighted the potential for single nucleotide polymorphism (SNP) detection (Fig. S6†). Performance of TMSDR with DNA as well as RNA target and working in VTM diluted in viral lysis buffer demonstrates point of care applicability of the assay (Fig. S7†). Compared to other isothermal amplification techniques such as HCR, the optimized TMSDR system demonstrated reduced background noise and efficient target recycling, leading to improved sensitivity and specificity.[32] Furthermore, TMSDR assay can also be conducted at lower and higher temperatures showcasing the stability of the assay (Fig. 5). While further optimization is needed to enhance the limit of detection and expand its applicability to diverse targets and sample types, this study establishes a robust foundation for the development of simple, cost-effective, and portable diagnostic tools based on TMSDR amplification.

Author contributions

J. B. K., J. D. and J. P. conceived and designed the study. J. B. K. carried out all the necessary experiments, data collection and data analysis. J. P., J. D. and J. B. K. participated in discussions and provided constructive feedback. J. B. K.,

J. P. and J. D. critically reviewed and revised the manuscript. All authors approved the final version of the manuscript.

Data availability

The raw data is submitted as ESI† (excel file with each sheet representing raw data for the curves illustrated in the main figures of the article).

Conflicts of interest

Galenvs sciences is an oligonucleotide supplier. Moreover, some of the work presented in the manuscript was used to file a provisional patent.

Acknowledgements

This work was supported by Mitacs accelerate grant. Authors also wish to thank Dr Adam Katolik for fruitful discussion regarding oligonucleotide purification.

References

1 L. Tang, T. Luo, S. Fan, Y. Liu and J. Song, *Biomater. Sci.*, 2023, **11**, 5060–5077.
2 S. Li, D. Zhao, F. Yang and S. Liu, *Chem. Commun.*, 2024, **60**, 570–573.
3 C. Chen, J. Wen, Z. Wen, S. Song and X. Shi, *Front. Genet.*, 2023, **14**, 1120791.
4 C. Chen, H. Wang, E. Zhu, X. Shi and J. Xu, *IEEE Access*, 2020, **8**, 88108–88114.
5 G. Xu, M. Lai, R. Wilson, A. Glidle, J. Reboud and J. M. Cooper, *Microsyst. Nanoeng.*, 2019, **5**, 37.
6 F. C. Simmel, B. Yurke and H. R. Singh, *Chem. Rev.*, 2019, **119**, 6326–6369.
7 Y. Liu, Y. Shi, K. Ding, J. Liu, H. Wang and H. Zhou, *Sens. Actuators, B*, 2023, **385**, 133655.
8 M. Mohammadniaei, M. Zhang, J. Ashley, U. B. Christensen, L. J. Friis-Hansen, R. Gregersen, J. G. Lisby, T. L. Benfield, F. E. Nielsen, J. Henning Rasmussen, E. B. Pedersen, A. C. R. Olinger, L. T. Kolding, M. Naseri, T. Zheng, W. Wang, J. Gorodkin and Y. Sun, *Nat. Commun.*, 2021, **12**, 5089.
9 Z. Zhao, Z. Chen, D. Liu, L. Wang and S. Liu, *Biosens. Bioelectron.*, 2021, **171**, 112706.
10 D. Y. Zhang and E. Winfree, *J. Am. Chem. Soc.*, 2009, **131**, 17303–17314.
11 T. Mayer, L. Oesinghaus and F. C. Simmel, *J. Am. Chem. Soc.*, 2023, **145**, 634–644.
12 K. J. Souza and D. K. Agrawal, *Med-X*, 2024, **2**, 1.
13 J. Xu, X. Han, W. Xu, J. Liu, A. Zhu, D. Song and F. Long, *Talanta*, 2023, **259**, 124475.
14 R. Augustine, A. Hasan, S. Das, R. Ahmed, Y. Mori, T. Notomi, B. D. Kevadiya and A. S. Thakor, *Biology*, 2020, **9**(8), 182.
15 M. N. Aoki, B. de Oliveira Coelho, L. G. B. Góes, P. Minoprio, E. L. Durigon, L. G. Morello, F. K. Marchini, I. N. Riediger, M. do Carmo Debur, H. I. Nakaya and L. Blanes, *Sci. Rep.*, 2021, **11**, 9026.
16 S. Leonardo, A. Toldrà and M. Campàs, *Sensors*, 2021, **21**(2), 602.
17 S. A. Bustin and T. Nolan, *Int. J. Mol. Sci.*, 2020, **21**(8), 3004.
18 G. Alhamid, H. Tombuloglu and E. Al-Suhaimi, *Sci. Rep.*, 2023, **13**, 5066.
19 J. B. Kapadia, N. Kharma, A. N. Davis, N. Kamel and J. Perreault, *RNA*, 2022, **28**, 263–273.
20 D. Wang, W. Tang, X. Wu, X. Wang, G. Chen, Q. Chen, N. Li and F. Liu, *Anal. Chem.*, 2012, **84**, 7008–7014.
21 S. Ding, X. Yu, Y. Zhao and C. Zhao, *Anal. Chim. Acta*, 2023, **1242**, 340810.
22 D. A. Khodakov, A. S. Khodakova, D. M. Huang, A. Linacre and A. V. Ellis, *Sci. Rep.*, 2015, **5**, 8721.
23 A. Akay, H. N. Reddy, R. Galloway, J. Kozyra and A. W. Jackson, *Heliyon*, 2024, **10**, e28443.
24 S. Khare, C. Gurry, L. Freitas, M. B. Schultz, G. Bach, A. Diallo, N. Akite, J. Ho, R. T. Lee, W. Yeo, G. C. Curation Team and S. Maurer-Stroh, *China CDC Wkly.*, 2021, **3**, 1049–1051.
25 S. Elbe and G. Buckland-Merrett, *Global Challenges*, 2017, **1**, 33–46.
26 A. R. Gruber, R. Lorenz, S. H. Bernhart, R. Neuböck and I. L. Hofacker, *Nucleic Acids Res.*, 2008, **36**, W70–W74.
27 P. Kerpedjiev, S. Hammer and I. L. Hofacker, *Bioinformatics*, 2015, **31**, 3377–3379.
28 F. C. Simmel, B. Yurke and H. R. Singh, *Chem. Rev.*, 2019, **119**, 6326–6369.
29 D. Y. Zhang and G. Seelig, *Nat. Chem.*, 2011, **3**, 103–113.
30 F. E. Marino, E. Proffitt, E. Joseph and A. Manoharan, *PLoS One*, 2022, **17**, e0266703.
31 H. Bui, V. Miao, S. Garg, R. Mokhtar, T. Song and J. Reif, *Small*, 2017, **13**, 1602983.
32 S. Li, P. Li, M. Ge, H. Wang, Y. Cheng, G. Li, Q. Huang, H. He, C. Cao, D. Lin and L. Yang, *Nucleic Acids Res.*, 2020, **48**, 2220–2231.
33 B. Wang, C. Thachuk, A. D. Ellington, E. Winfree and D. Soloveichik, *Proc. Natl. Acad. Sci. U. S. A.*, 2018, **115**, E12182–E12191.